Modulation mixing in a multimode dye laser

Karl Koch, Stephen H. Chakmakjian, Stephanos Papademetriou, and C. R. Stroud, Jr.
The Institute of Optics, University of Rochester, Rochester, New York 14627
(Received 22 December 1988)

We use an argon-ion laser, modulated at two or more frequencies, to pump a multimode dye laser. Time series of the modulated pump and the output of the dye laser are collected simultaneously. The dye-laser response is analyzed for the presence of chaotic and quasiperiodic attractors. We estimate and compare the correlation dimension and the order-2 Renyi entropy of both the modulated-pump and dye-laser output signals using an embedding-space technique. Fourier transforms of the time series are also compared.

I. INTRODUCTION

The behavior of a nonlinear system under the influence of multiple driving frequencies has been the subject of a number of recent publications.[1–7] Numerical simulations by Pomeau *et al.*[1] examine a two-level atom illuminated by two fields of different frequencies. The authors find that when the two frequencies are commensurate (i.e., the ratio of the two frequencies is a rational number), the system exhibits a periodic response. In contrast, when the two frequencies are incommensurate (i.e., the ratio of the two frequencies is an irrational number), the system exhibits a more complicated response; the Fourier transform of the time series of the inversion is broadband and the wave function's time-dependent autocorrelation function falls off rapidly. These results suggest that a conservative system driven at two incommensurate frequencies may behave chaotically. However, the numerical simulations of Eidson and Fox[2] show that if one approximates an incommensurate ratio by a ratio of small integers, the spectrum of the atomic response can clearly be resolved into combination tones of the two frequencies. When the incommensurate ratio is approximated by a ratio of larger integers, the time necessary for resolving the combination tones increases. This could be the reason broadband spectra were observed in Ref. 1. In addition, numerical calculations by Badii and Meier[3] show that a double Poincaré section of the inversion's time series yields a smooth curve indicating the motion is, although quite complicated, quasiperiodic. The conclusion of these works suggests that a conservative system driven by two incommensurate frequencies is not chaotic. The experimentally important complication of dissipation in the dynamics of the system has not been addressed in Refs. 1–3. Many systems that do not exhibit chaos in a conservative framework become chaotic when damping mechanisms are added to the dynamics.

In work concerning incommensurate frequencies in dissipative nonlinear systems, Hopf[4] considers the propagation of a quasiperiodic field, modulated in amplitude and phase, through an inhomogeneously broadened amplifier. Reference 4 finds that embedding techniques[8] classify the output of the amplifier as noise; although arguments are made to suggest that chaos is not necessarily excluded. However, it is not clear whether the time series analyzed were long enough to resolve the combination tones generated in the field on propagating through the amplifier.

The interaction of multiple-frequency fields is also of interest in considering Landau's proposal for a possible mechanism for the onset of turbulence. Landau proposed that, as a parameter of the system was varied, the spectrum of the system would successively develop incommensurate frequencies, along with combination tones of the existing frequencies, until the system's behavior becomes quite complicated or turbulent. In contrast to this route to turbulence, Ruelle and Takens[9] and Newhouse *et al.*[10] predict that multifrequency quasiperiodic motion is unstable to perturbative changes of the system. These perturbative changes in the system convert the quasiperiodic motion to chaotic motion. However, a numerical study of three- and four-frequency quasiperiodic maps by Grebogi *et al.*[6,7] shows that stable three- and four-frequency quasiperiodic orbits are possible. Three-frequency quasiperiodic orbits have been observed experimentally.[11,12] Unlike the work presented here, these experimental three-frequency quasiperiodic orbits arose from three Hopf bifurcations in the dynamic response of the system; in this experiment we externally drive the system at two or more frequencies.

The experimental investigation of a dissipative nonlinear system driven by multiple frequencies is the subject of this paper. The output power of a laser is a nonlinear function of the pump power near the threshold for lasing. Other nonlinear effects such as discontinuous intensity jumps, hysteresis, and the effects of critical slowing down can be observed in the output power of lasers. The high-Q multimode ring dye laser used in previous experiments[13] has displayed all of these effects. The nonlinear kink at the threshold for lasing, discontinuous intensity jumps, and hysteresis are seen in Fig. 1. The plot shows the dye-laser output power as a function of normalized pump power when the pump power is swept sinusoidally at 2 kHz. The abscissa in Fig. 1 is pump-power divided by threshold pump power. These nonlinearities provide the system with a mechanism for mixing the driving frequencies. The possibility of generating new frequencies or a chaotic response are also possible.

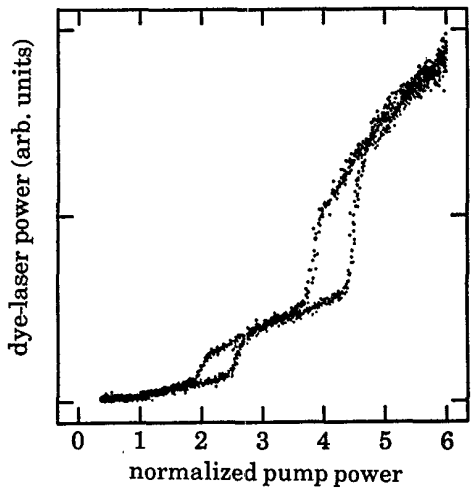

FIG. 1. Output power of the dye laser vs normalized pump power. The dye-laser-output power and modulated-pump power are simultaneously digitized as the pump power is swept sinusoidally at 2 kHz. The normalized pump power is defined as the pump power divided by the threshold pump power. For this dye-laser configuration the threshold pump power is approximately 1 W. The figure illustrates the severe nonlinear relationship that exists between the pump power and the dye-laser-output power.

Lasers are often used as pump sources for other lasers. The different modes of a multimode pump laser or the single modes of many individual pump lasers can beat together to form a modulation of the pump source. In this paper we study the effect the modulation has on the output of the laser being pumped. Specifically, we examine a multimode dye laser being pumped by an argon-ion laser with adjustable modulation frequencies. The results of this experimental work are not only relevant to the study of nonlinear systems driven by multiple frequencies, but also give information about the behavior of a multimode dye laser with a time-dependent pump parameter.

II. EXPERIMENTAL SETUP

The experimental setup is sketched in Fig. 2. A multimode argon-ion laser, operating at a single wavelength 5145 Å, is used to pump a multimode dye laser. The longitudinal mode spacing of the argon-ion laser is approximately 80 MHz. The rms amplitude of 80-MHz modulation is 0.2% of the total intensity. The rms amplitude of the line frequency and its harmonics is less than 1% of the total intensity. The beam of the argon-ion laser is focused through an acousto-optic modulator. The zeroth-order output of the modulator is recollimated before being focused on the dye jet of the dye laser. We found it necessary to focus and recollimate to preserve the TEM_{00} beam and to maximize the bandwidth from the modulator. The bandwidth of this modulation was approximately 4 MHz. The acousto-optic modulator is driven by a 40-MHz radio-frequency source. The amplitude of the 40-MHz signal is modulated by the sum of a series of oscillators. The oscillators are operated from 1 to 400 kHz.

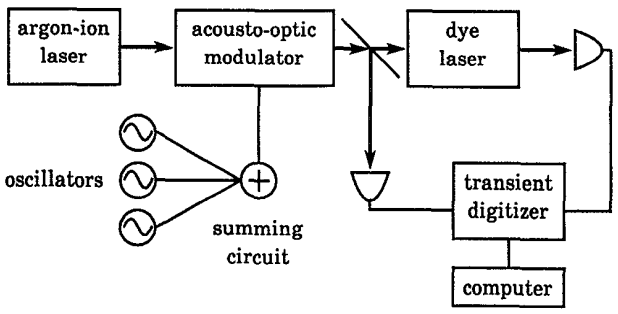

FIG. 2. Schematic diagram of the experimental setup. The argon-ion laser beam is passed through an acousto-optic modulator. The modulator is driven by the sum of a series of sinusoidal oscillators. The zeroth-order output of the modulator and the output of the dye laser are simultaneously recorded with a transient digitizer. A computer is used for analyzing the time series.

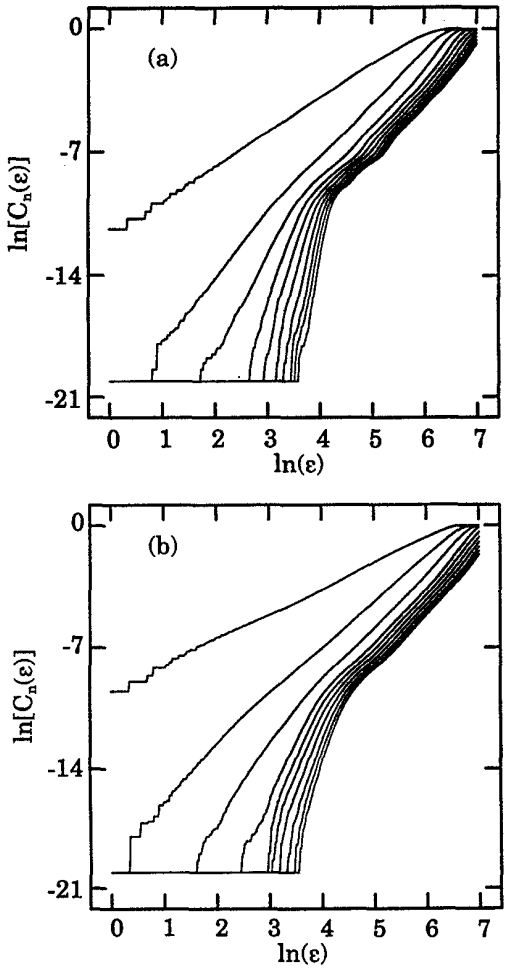

FIG. 3. The number of vector pairs within ϵ vs $\ln(\epsilon)$ for even embedding dimensions from 2 to 20. We normalize the number of vector pairs by the total number of pairs. The pump is modulated at three commensurate frequencies. (a) Results for modulated-pump time series. (b) Results for the dye-laser-output time series.

The contrast ratio (maximum-minimum)/(maximum +minimum), of the total intensity of the pump laser is varied between 0.90 and 0.50 in the experiments. These contrast ratios are sufficient to bring the dye laser below threshold and 5–6 times above threshold. The dye laser is similar to the lasers used in previous experiments.[13] All the mirrors are broadband high reflectors. A Brewster-angle quartz prism is used for frequency selection. The time-averaged linewidth of the dye laser is approximately 1 Å. The zeroth-order output of the acousto-optic modulator is monitored using a beam splitter and photodiode. The output of the dye laser is also monitored using a *p-i-n* photodiode. The response of the photodiodes drops to one half of the low-frequency response at 8 MHz. We record the signals from the photodiodes using a 10-bit transient digitizer. The transient digitizer simultaneously samples the two photodiodes every 200 nsec. Series of 2^{15} points are transferred to a computer for analysis.

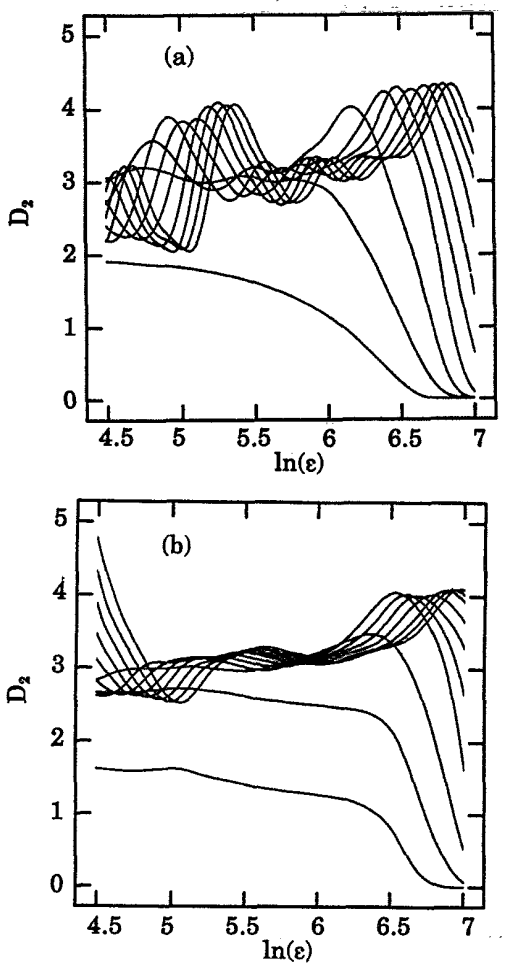

FIG. 4. (a) The results of a 13-point linear regression on the data in Fig. 3(a). The slopes of the curves in Fig. 3(a) are plotted as a function of $\ln(\epsilon)$. (b) The results of a 13-point linear regression on the data in Fig. 3(b). The slopes of the curves in Fig. 3(b) are plotted as a function of $\ln(\epsilon)$. The slopes of both sets of curves converge to approximately the same value for D_2. Only the even embedding dimensions from 2 to 20 are plotted.

III. EXPERIMENTAL ANALYSIS

We use a method developed by Grassberger and Procaccia[8] to analyze our data for the presence of deterministic noise and the generation of new frequency components. The method takes a one-dimensional time series $x(t_i)$ and forms vectors in an embedding space of dimension n. The vectors have elements $x(t_i)$, $x(t_i+\tau)$, $x(t_i+2\tau),\ldots,x(t_i+(n-1)\tau)$. We choose τ by calculating the first maxima in the area covered by a plot of $x(t_i)$ versus $x(t_i+\tau)$.[14] The number of n-dimensional vector pairs whose ends are within a distance ϵ, $C_n(\epsilon)$, is determined as a function of ϵ and n. In the limit that ϵ approaches zero and n approaches infinity, $C_n(\epsilon)$ scales as

$$C_n(\epsilon)\propto\epsilon^{D_2}\exp(-nK_2\tau)\ , \tag{1}$$

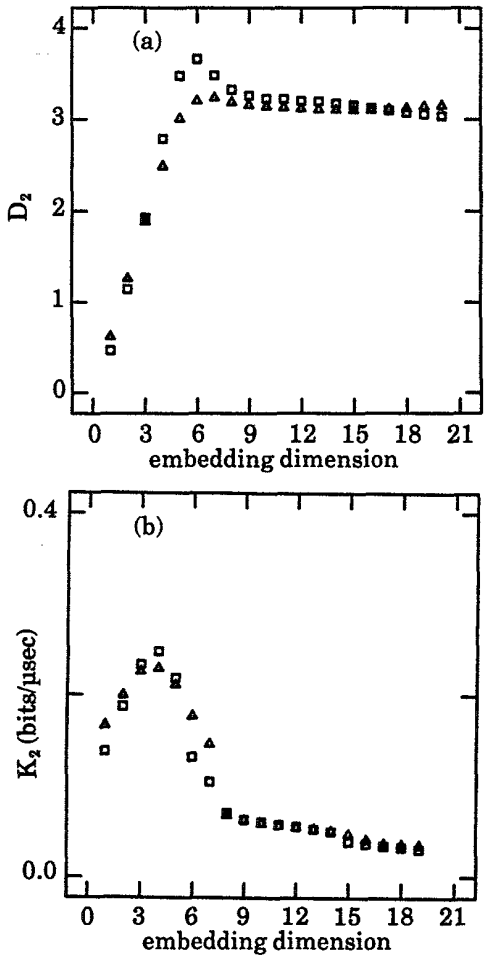

FIG. 5. D_2 and K_2 as a function of embedding dimension for commensurate driving frequencies. (a) D_2 as a function of embedding dimension. The value of D_2, averaged over the region of convergence in Fig. 4, is plotted as a function of embedding dimension. (b) K_2 as a function of embedding dimension. The value of K_2, averaged over the same region as in 5(a), is plotted as a function of embedding dimension. Embedding dimensions from 1 to 20 are plotted. The squares (triangles) represent the data for the modulated-pump (dye-laser-output) time series.

where D_2 is the correlation dimension of the attractor and K_2 is the order-2 Renyi entropy. The order-2 Renyi entropy is a lower bound of the Kolmogorov entropy of the system. It has been shown[8] that K_2 is zero for a periodic system, infinite for a stochastic system, and finite but nonzero for a chaotic system. Taking the logarithm of both sides of Eq. (1) gives

$$\ln[C_n(\epsilon)]=D_2\ln(\epsilon)-nK_2\tau+c\ , \tag{2}$$

where c is an arbitrary constant. In practice one plots $\ln[C_n(\epsilon)]$ as a function of $\ln(\epsilon)$ for a series of embedding dimensions n. So, in the limit of large n and small ϵ, the curves approach straight lines with slope D_2. The distance between the straight lines of successive embedding dimensions gives $K_2\tau$. We calculate $C_n(\epsilon)$ from embedding dimensions of 1 to 20. The magnitude of our data ranges from 0 to 1023. Since the data are strictly integers, there is no information below $\epsilon=1$. If ϵ is large enough to contain all the ends of the vectors, no information is gained by making ϵ any larger. So we choose the parameter ϵ to run from 1 to 1500. We calculate $C_n(\epsilon)$ for 400 equally spaced values of $\ln(\epsilon)$. We then use a 13-point linear-regression analysis to calculate the slopes of the curves as a function of ϵ. The 13-point linear regression calculates the slope of a best-fit straight line for each group of 13 points along the $\ln(\epsilon)$ axis. Then we plot the calculated slopes as a function of $\ln(\epsilon)$. The slopes of the curves converge to D_2, the correlation dimension of the system, for large embedding dimension. The region of ϵ where the slopes converge is used to calculate K_2. We plot D_2 and K_2 as a function of embedding dimension to extrapolate their large embedding-dimension values.

Some simple examples of well-characterized time series were used to test the numerical algorithm of the Grassberger-Procaccia method. The time series of one of the dimensions of the Hénon map[15] with parameters $a=1.4$ and $b=0.3$ gives a correlation dimension of 1.19 and a K_2 of 0.42 bits/iteration in agreement with values in the literature.[8,16] A single-frequency sine wave of 10 kHz, sampled every 1.6 μsec with a 10-bit accuracy, is

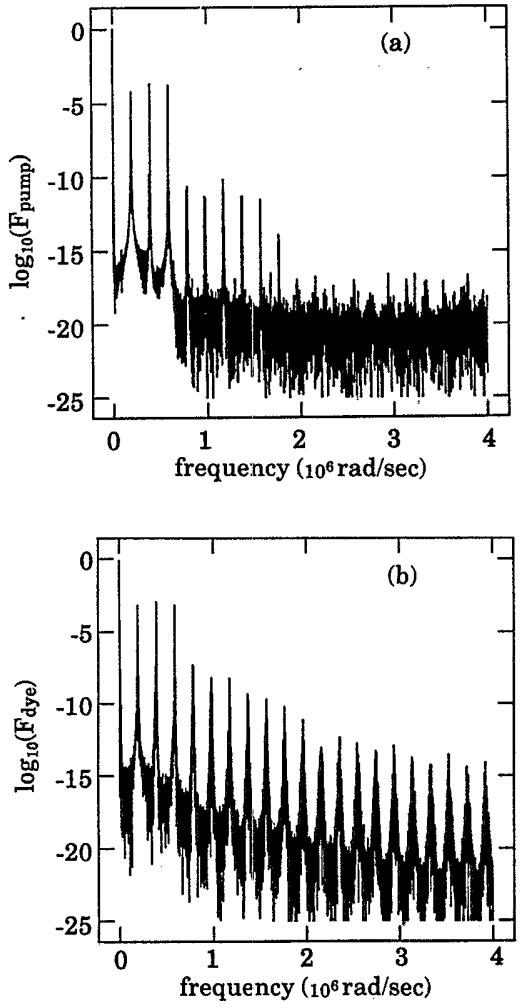

FIG. 6. Fourier transform of the time series for commensurate driving frequencies. (a) Fourier transform of the modulated-pump time series as a function of frequency. (b) Fourier transform of the dye-laser-output time series as a function of frequency.

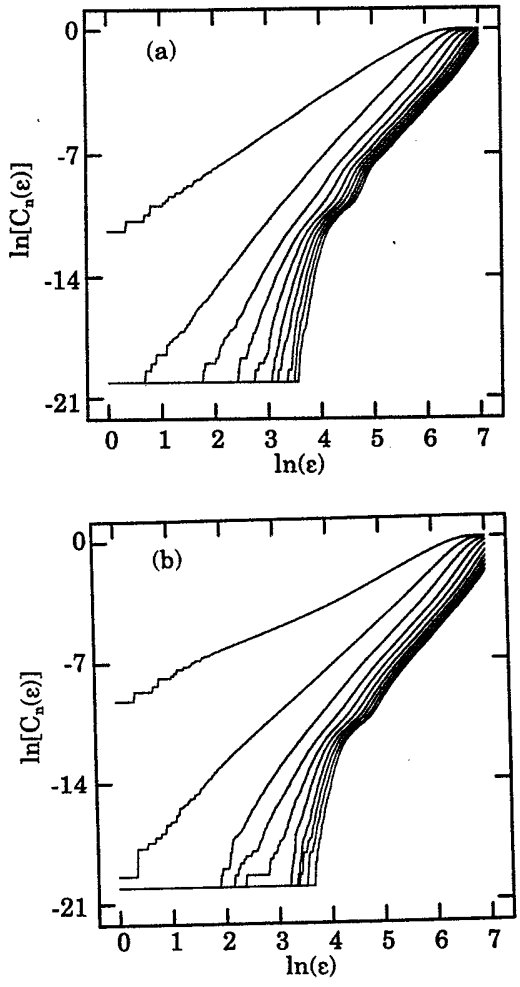

FIG. 7. Number of vector pairs within ϵ vs $\ln(\epsilon)$ for even embedding dimensions from 2 to 20. We normalize the number of vector pairs by the total number of pairs. The pump is modulated at three incommensurate frequencies. (a) Results for modulated-pump time series. (b) Results for the dye-laser-output time series.

found to have a correlation dimension of 1.0 and a K_2 of less than 0.1 bits/period. Since there is one frequency in the system, the results for the correlation dimension agree with what is expected. The somewhat large value of K_2 is a result of random noise in the digitization of the sine wave. The sum of two sine waves of incommensurate frequencies $[\omega_1/2\pi=10$ kHz and $\omega_2=\omega_1(1+\sqrt{5})/2]$, is found to have a correlation dimension of 2.1 and a K_2 of less than 0.2 bits/period. The correlation dimension has increased with the number of incommensurate frequencies. We then analyzed the square of the sum of two sine waves of incommensurate frequencies ω_1 and ω_2. The square of the sum generates four frequencies: $2\omega_1$, $2\omega_2$, $\omega_1+\omega_2$, and $\omega_1-\omega_2$. Each pair of frequencies is incommensurate, which might lead one to conclude that there are four incommensurate frequencies; however, the correlation dimension for this time series is equal to 2.0. Therefore, we conclude that the correlation dimension scales with the number of linearly independent frequencies. This definition has been used in previous studies with multifrequency fields.[5-7] The value of K_2 for this time series approaches 0.2 bits/period. Consequently, this method of data analysis allows us to distinguish a spectrum of combination tones from a spectrum where new independent frequency components have been created. If the correlation dimension increases, we know new linearly independent frequency components have been created. Since a change in the value of K_2 signifies a change in the system's information, we also expect a corresponding change in the value of K_2 for the time series with new linearly independent frequencies. If the correlation dimension and the order-2 Renyi entropy decrease or remain the same, then we conclude that no new linearly independent frequency components have been created.

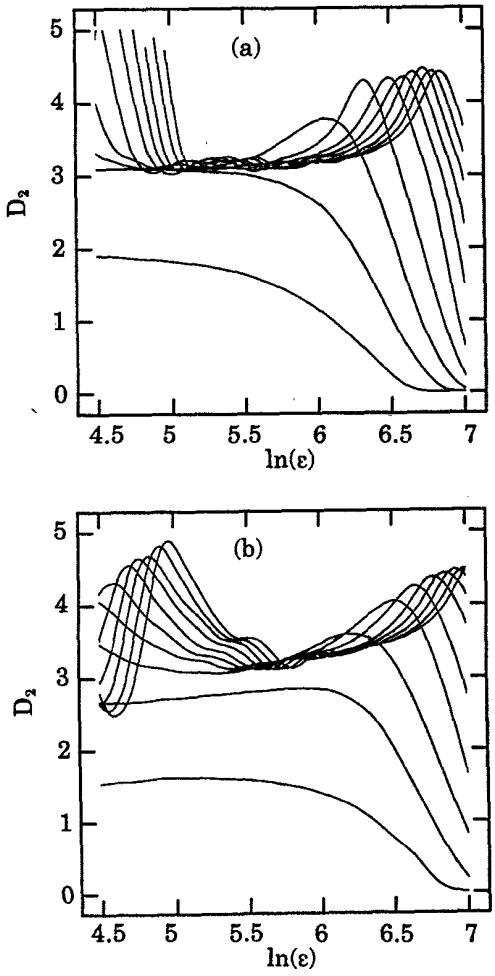

FIG. 8. (a) Results of a 13-point linear regression on the data in Fig. 7(a). The slopes of the curves in Fig. 7(a) are plotted as a function of $\ln(\epsilon)$. (b) The results of a 13-point linear regression on the data in Fig. 7(b). The slopes of the curves in Fig. 7(b) are plotted as a function of $\ln(\epsilon)$. The slopes of both sets of curves converge to approximately the same value for D_2. Only the even embedding dimensions from 2 to 20 are plotted.

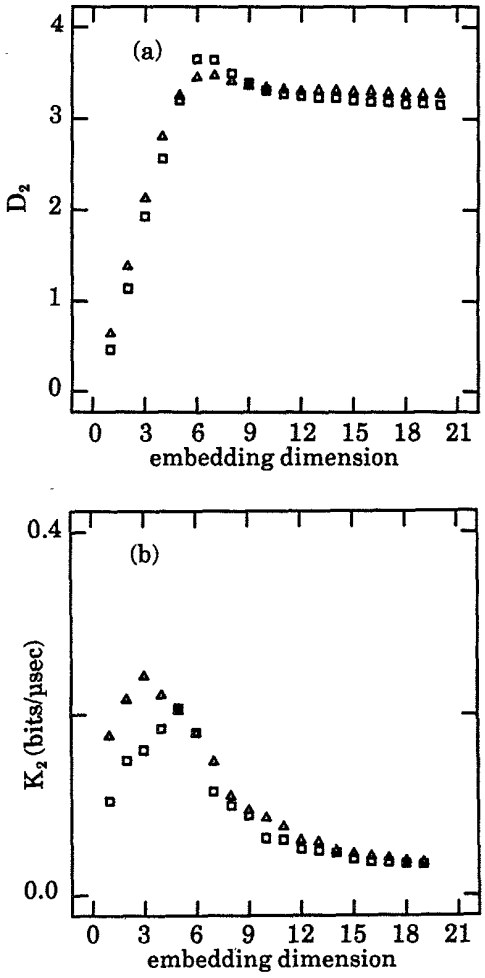

FIG. 9. D_2 and K_2 as a function of embedding dimension for incommensurate driving frequencies. (a) D_2 as a function of embedding dimension. The value of D_2, averaged over the region of convergence in Fig. 8, is plotted as a function of embedding dimension. (b) K_2 as a function of embedding dimension. The value of K_2 averaged over the same region as in (a), is plotted as a function of embedding dimension. Embedding dimensions from 1 to 20 are plotted. The squares (triangles) represent the data for the modulated-pump (dye-laser-output) time series.

IV. EXPERIMENTAL RESULTS

We have carried out experiments where the pump modulation consists of one, two, three, or four frequencies. When a single frequency modulates the pump beam, the dye laser responds at the harmonics of the modulation frequency. The results obtained for two- and three-frequency modulations of the pump beam show the dye laser responds at the harmonics and combination tones of the applied modulation frequencies.

In Fig. 3(a) we plot $\ln[C_n(\epsilon)]$ as a function of $\ln(\epsilon)$ for the time series of the pump modulated at three commensurate frequencies. In Fig. 3(b) we plot $\ln[C_n(\epsilon)]$ as a function of $\ln(\epsilon)$ for the time series of the dye-laser output. Figures 4(a) and 4(b) show the results of a 13-point linear regression analysis on the curves in Fig. 3(a) and 3(b), respectively. In both cases the slopes of the lines converge in the limit of large embedding dimension. The value for D_2 is obtained by averaging the results of the 13-point linear regression over the region of ϵ where the slopes converge. In Fig. 5(a) we plot the correlation dimension D_2 as a function of embedding dimension for the modulated-pump time series (squares) and the dye-laser-output time series (triangles). Figure 5(b) is a plot of K_2 as a function of embedding dimension for the modulated-pump time series (squares) and the dye-laser-output time series (triangles). The value for K_2 is obtained in the same region of ϵ as the correlation dimension in Fig. 5(a). The Fourier transforms of the modulated-pump time series and the dye-laser-output time series F_{pump} and F_{dye} are plotted in Figs. 6(a) and 6(b), respectively. Since both signals are made up of well-resolved harmonics, the signals are expected to be periodic. We know that the modulated-pump time series is strictly periodic and therefore K_2 is zero. We can interpret any deviation from zero as an indication of stochastic noise in the detection or an anomaly of the technique we are using to analyze the data. In Fig. 5(b) any deviation in K_2 for the two time series indicates the dye-laser output is not periodic and has developed chaotic or stochastic noise in excess of that on the modulated pump. Figure 5(b) indicates that for commensurate modulation frequencies the dye laser is still periodic since K_2 is identical for the two time series.

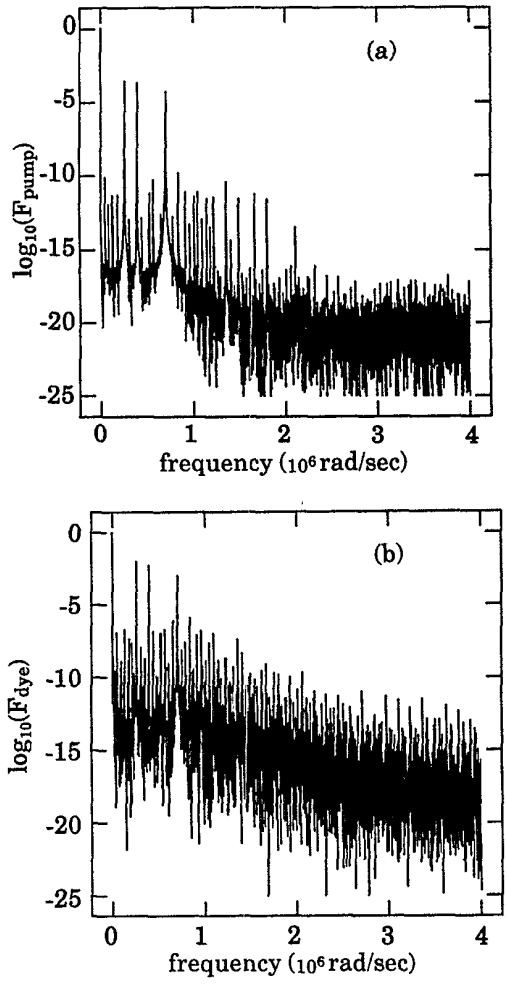

FIG. 10. Fourier transform of the time series for incommensurate driving frequencies. (a) Fourier transform of the modulated-pump time series as a function of frequency. (b) Fourier transform of the dye-laser-output time series as a function of frequency.

In Fig. 7(a) we plot $\ln[C_n(\epsilon)]$ as a function of $\ln(\epsilon)$ for the time series of the pump modulated at three incommensurate frequencies. The choice of incommensurate frequencies was made while monitoring the spectrum of the dye laser using an rf spectrum analyzer. One oscillator remained fixed in frequency, while the frequencies of the other oscillators were varied until a broadband spectrum was observed. Figure 7(b) is a plot of $\ln[C_n(\epsilon)]$ as a function of $\ln(\epsilon)$ for the time series of the dye-laser output. The results of a 13-point linear regression on the curves in Figs. 7(a) and 7(b) are shown in Figs. 8(a) and 8(b), respectively. Again in both cases the slopes converge in the limit of large embedding dimension. In Fig. 9(a) we plot the correlation dimension D_2 as a function of embedding dimension for the modulated-pump time series (squares) and the dye-laser-output time series (triangles). The values for D_2 were obtained in a manner similar to those in Fig. 5(a). Figure 9(b) is a plot of K_2 as a function of embedding dimension for the modulated-pump time series (squares) and the dye-laser-output time series (triangles). The Fourier transforms of the modulated-pump time series and the dye-laser-output time series F_{pump} and F_{dye} are plotted in Figs. 10(a) and 10(b), respectively. While the spectrum in Fig. 10(a) is a finite series of discrete components, the spectrum of Fig. 10(b) is a broadband spectrum. However, from Figs. 9(a) and 9(b) we see the values of D_2 and K_2 that the dye-laser-output time series converges to are identical to those of the modulated-pump time series. We can conclude that since the correlation dimension D_2 is identical for both time series that no new independent frequency components have been created and the spectrum of the dye-laser output is composed purely of combination tones of the modulated-pump spectrum. This indicates that even though the dye-laser output is quite complicated, it is merely quasiperiodic.

Similar experiments were carried out for two-, three-,

and four-frequency modulations. The frequencies were varied in the range of 1 to 400 kHz. The results of these other experiments are similar to the results of the three-frequency modulation discussed above. In all cases no chaos was detected in the output of the dye laser.

V. CONCLUSION

We find that the correlation dimension of a system scales with the number of linearly-independent frequencies. This fact allows us to separate broadband spectra which are truly broadband from broadband spectra which are dense spectra of combination tones. These conclusions were facilitated by careful use of an embedding-space technique developed by Grassberger and Procaccia.[8] It should also be noted that if shorter time series were used in the analysis, the slopes of the curves, $C_n(\epsilon)$ versus ϵ, did not converge. The embedding space technique classifies such time series as noise. It is interesting to note that a Fourier transform of the truncated time series would not resolve the combination tones in the dye-laser spectrum. The embedding technique, however, is much more convenient than a Fourier transform for distinguishing truly broadband spectra from complicated spectra of combination tones.

We show that the output of a multimode dye laser, driven by a modulated pump, exhibits broadband spectral features which are simply combination tones of the pump-source modulation frequencies. This indicates the mechanism responsible for the broadband spectrum generates new frequencies from combination tones of the existing frequencies. Phase-matched four-wave mixing is a simple example of how these new frequencies might be generated. The large depth of pump modulation makes it possible for higher-order mixings to become of comparable significance as well.

We also demonstrate that the high-Q multimode ring dye laser has stable multifrequency quasiperiodic attractors for two, three, and four incommensurate driving frequencies. These results are similar to the results of Grebogi *et al.*[6,7] The absence of chaos in this system is somewhat surprising given the extreme nonlinearities of the system which are illustrated in Fig. 1. A partial answer to this puzzle lies in the fact that the hysteresis loops observed in Fig. 1 do not remain stable for multifrequency pumping. The transition points of the hysteresis loop do not remain fixed. This is related to critical slowing down that takes place at this second instability threshold. Clearly, further study of this phenomena will be very important in completely understanding the results of this experiment.

ACKNOWLEDGMENTS

We wish to thank Dan Gauthier for computer programs of the Grassberger-Procaccia method and helpful discussions of their results. We also acknowledge the support of the University Research Initiative through the Center for Opto-Electronic Research.

[1]Y. Pomeau, B. Dorizzi, and B. Grammaticos, Phys. Rev. Lett. **56**, 681 (1986).
[2]J. Eidson and R. F. Fox, Phys. Rev. A **34**, 3288 (1986).
[3]R. Badii and P. F. Meier, Phys. Rev. Lett. **58**, 1045 (1987).
[4]F. A. Hopf, Phys. Rev. Lett. **56**, 2800 (1986).
[5]C. Grebogi, E. Ott, S. Pelikan, and J. A. Yorke, Physica **13D**, 261 (1984).
[6]C. Grebogi, E. Ott, and J. A. Yorke, Phys. Rev. Lett. **51**, 339 (1983).
[7]C. Grebogi, E. Ott, and J. A. Yorke, Physica **15D**, 354 (1985).
[8]P. Grassberger and I. Procaccia, Phys. Rev. A **28**, 2591 (1983).
[9]D. Ruelle and F. Takens, Commun. Math. Phys. **20**, 167 (1971).
[10]S. Newhouse, D. Ruelle, and F. Takens, Commun. Math. Phys. **64**, 35 (1978).
[11]A. Libchaber, S. Fauve, and C. Laroche, Physica **7D**, 73 (1983).
[12]S. Martin, H. Leber, and W. Martienssen, Phys. Rev. Lett. **53**, 303 (1984).
[13]L. W. Hillman, J. Krasinski, R. W. Boyd, and C. R. Stroud, Jr., Phys. Rev. Lett. **52**, 1605 (1984); C. R. Stroud, Jr., K. Koch, and S. H. Chakmakjian, in *Optical Instabilities,* edited by R. W. Boyd, M. G. Raymer, and L. M. Narducci (Cambridge University, Cambridge, England, 1986), pp. 274–276. C. R. Stroud, Jr., K. Koch, S. H. Chakmakjian, and L. W. Hillman, in *Optical Chaos,* edited by J. Chrostowski and N. B. Abraham, Proc. SPIE **667**, 47 (1986).
[14]A. M. Fraser and H. L. Swinney, Phys. Rev. A **33**, 1134 (1986).
[15]M. Hénon, Commun. Math. Phys. **50**, 69 (1976).
[16]A. Wolf, J. B. Swift, H. L. Swinney, and J. A. Vastano, Physica **16D**, 285 (1985).